Aeolian Research 21 (2016) 93–107

Contents lists available at ScienceDirect

Aeolian Research

journal homepage: www.elsevier.com/locate/aeolia

Climatology of dust distribution over West Asia from homogenized remote sensing data

Seyed Omid Nabavi [a,*], Leopold Haimberger [a,1], Cyrus Samimi [b,c,2]

[a] Department of Meteorology and Geophysics, University of Vienna, Faculty of Earth Sciences, Geography and Astronomy, UZA II Althanstrasse 14, A-1010 Vienna, Austria
[b] Faculty of Biology, Chemistry and Earth Sciences, University of Bayreuth, Universitätsstr. 30, 95447 Bayreuth, Germany
[c] Bayreuth Center of Ecology and Environmental Research, BayCEER, Dr. Hans-Frisch-Straße 1-3, 95448 Bayreuth, Germany

ARTICLE INFO

Article history:
Received 28 October 2015
Revised 30 March 2016
Accepted 4 April 2016
Available online 13 April 2016

Keywords:
Dust storms
TOMS-OMI Aerosol Index
MODIS
SeaWIFS
West Asia

ABSTRACT

In the past decade, West Asia has witnessed more frequent and intensified dust storms affecting Iran and Persian Gulf countries. Employing a varying threshold that takes into account systematic differences between TOMS and OMI data, TOMS-OMI Aerosol Index data are used to identify long-term changes in the horizontal distribution of dust storms in West Asia from 1980 to present. The northwest of Iraq and east of Syria are identified as emerging dusty areas, whereas east of Saudi Arabia and southeast of Iraq are identified as permanent dusty areas, including both dust sources and affected areas. Whereas the frequency of dust events increased slightly in the permanent dusty areas, it increased markedly in the emerging dusty areas. As expected, the frequency of dust events is highest in June and July.

The dust source areas are identified as the Iraq-Saudi Arabia boundary region and (recently) the northwest of Iraq, using MODIS deep blue aerosol optical depth data. Subsequently, a lagged correlation was implemented between identified dust sources and whole West Asia to determine the main paths and receptors of intense dust storms. Accordingly, southwest of Iran and Persian Gulf countries were determined as main receptors of summertime dust storms in West Asia. During spring, dust storms mostly hit the northern half of the region and reach to the Caspian Sea. Analyzing atmospheric patterns, Shamal and Frontal patterns were found as dominant atmospheric circulations simultaneous with summertime and springtime dust storms, respectively.

1. Introduction

Dust storms are known as a natural hazard that affects various parts of the world. According to the definition of World Meteorological Organization (WMO), dust storms are the result of strong atmospheric turbulence near the surface that lifts large amounts of dust into the atmosphere, which decrease the horizontal visibility to less than 1000 m (Goudie and Middleton, 2006). Reduction in visibility range leads to vehicle accidents. Reduction of soil productiveness, damages to agricultural products, remote communication disturbances, mechanical systems disorders (Jish Prakash et al., 2014), higher risk of respiratory diseases (Lyles et al., 2012; Ebrahimi et al., 2014) are also consequences of dust storms. In a general perspective, primary origins of dust storms are located in the world's arid regions in East Asia, Middle East, Europe, Latin America, North America, Australia, east and south of Africa, and Sahara. The Middle East has various dust source areas such as the Arabian Peninsula, Israel, Syria, Egypt, Iraq and Iran (Shao et al., 2011). In the past years, dust events have been more frequent and intensified in West Asia (Azizi et al., 2012).

1.1. Remotely sensed dust data

In order to mitigate dust disastrous effects, monitoring its sources, transport paths and affected areas is crucial (Ciren and Kondragunta, 2014). Unfortunately almost all Middle East countries have incomplete ground-based observation datasets which are largely limited to urban areas. Meanwhile, remote sensing tools and techniques potentially provide an unprecedented capability to monitor the spatial–temporal distribution of dust events. Many algorithms have been developed to detect dust events from other atmospheric phenomena and ground surface features. Ackerman (1989) proposed brightness temperature difference (BTD) between

* Corresponding author. Tel.: +43 1 4277 537 01; fax: +43 1 4277 95 37.
E-mail addresses: seyed.omid.nabavi@univie.ac.at (S.O. Nabavi), leopold.haimberger@univie.ac.at (L. Haimberger), cyrus.samimi@uni-bayreuth.de (C. Samimi).
[1] Tel.: +43 1 4277 537 01; fax: +43 1 4277 95 37.
[2] Tel.: +49 921 552237.

http://dx.doi.org/10.1016/j.aeolia.2016.04.002
1875-9637/

near-infrared channels at 3.7 and 11 μm and, later (1997), a tri-spectral (8, 11 and 12 μm) technique to differentiate dust particles from water/ice clouds. However, Ciren and Kondragunta (2014) have mentioned that the magnitude of the brightness temperature difference is sensitive to the dust layer height and the dust composition and surface emissivity. Therefore, the accuracy of dust detection can vary both spatially and temporally. Due to the strong absorption of Ultra Violet (UV) radiance by dust and low ground surface reflectivity in the UV spectral region, an Aerosol Index (AI) has first been defined by Torres et al. (1998) for Total Ozone Mapping Spectrometer (TOMS) and Ozone Monitoring Instrument (OMI) UV radiances. AI is mathematically defined as:

$$\mathrm{AI} = \log_{10}(I_{360}/I_{331})_{\mathrm{measured}} - \log_{10}(I_{360}/I_{331})_{\mathrm{calculated}} \quad (1)$$

The "*I*" denotes radiance measured by TOMS and OMI at 360 nm and 331 nm wavelengths, respectively. Since $I_{360\ \mathrm{calculated}}$ is calculated using reflectivity derived from the 331 nm radiance values, the Aerosol Index definition essentially simplifies to:

$$\mathrm{AI} = \log_{10}(I_{360\mathrm{measured}}/I_{360\mathrm{calculated}}) \quad (2)$$

The AI can identify absorbing, smoke and desert, and non-absorbing, ice and water, aerosols. AI positive values are representative of mineral dust, smoke and volcanic aerosols (Ahmad et al., 2006). Using TOMS AI, Prospero et al. (2002) depicted globally major dust sources which are in topographic depressions of former paleolakes. While the TOMS AI seems ideal for climatological studies since it is available back to 1979, it also has its weaknesses. Mahowald and Dufresne (2004) have pointed out that AI is sensitive to dust layer height. Assuming a constant dust concentration, this means higher dust clouds lead to higher, exaggerated, AI values over desert areas and during warm periods of the year whereas dust is underestimated with AI during cooler periods and areas. Therefore, they have recommended using a spatiotemporally Varying Threshold (VT) for the detection of dust events, instead of direct use of AI or determining a Fixed Threshold (FT).

Although this can partly deal with dust height-induced biases, an AI binary mask is not able to show the severity of dust storms. Moreover, TOMS AI is prepared in the resolution of ≈1° which is too rough to identify local scale dust activity. This deficiency can be addressed by the use of high-resolution Moderate Resolution images of Imaging Spectroradiometer (MODIS). Hsu et al. (2004) developed a Deep Blue (DB) Aerosol Optical Depth (AOD) algorithm for MODIS images available from 2003 to 2014. This algorithm is not only insensitive to dust height but also able to detect dust over a bright surface, e.g., desert areas, at a high resolution of 10 km. Ginoux et al. (2012) have used this algorithm to identify anthropogenic and natural sources from MODIS aerosol products. Results show that the main sources of dust storms in West Asia are vast desert areas located in the northeast of Saudi Arabia, Iraq, Iran, Syria and the regions between the Caspian Sea and Aral Lake.

Besides MODIS, DB AOD data at 550 nm can also be prepared from measurements of Sea-viewing Wide Field-of-view Sensor (SeaWIFS). These data are accessible in two resolutions of 0.5° and 1° from 1998 to 2010. Hsu et al. (2012) have used this dataset to identify distribution and trends of aerosols in global and regional scales. Results show strong relationships between Saharan dust export as well as biomass-burning activity in the tropics with climate indices such as El Niño Southern Oscillation (ENSO).

1.2. Dust storms in West Asia

The significant increase of dust storms in West Asia (Azizi et al., 2012) has fostered studies based on various research approaches (Goudie and Middleton, 2000; Furman, 2003; Taghavi and Asadi, 2007; Aurelius et al., 2007; Al Sarraf, 2010; Gerivani et al., 2011; Hamidi et al., 2013; Rezazadeh et al., 2013; Cao et al., 2015; Moridnejad et al., 2015b; Rashki et al., 2015). Some of those studies have used the discussed remote sensing techniques and algorithms for the analysis of dust storms in the region (Esmaili et al., 2006; Azizi et al., 2012; Karimi et al., 2012; Boloorani et al., 2014; Moridnejad et al., 2015a). Although these studies have yielded valuable results, they left some issues to be addressed. Esmaili et al. (2006) have used TOMS AI and meteorological data to identify major dust sources of Iran. They took only the appearance of persistent spatial–temporal patterns of AI as the indicator of Iran's dust sources before 2004. Azizi et al. (2012) and (Boloorani et al., 2014) both have applied a BTD algorithm on MODIS images during some dust cases between 2000 and 2008. They have concluded that most dust storms entering Iran form in Iraq and Syria. Karimi et al. (2012) compared different dust detection algorithms to be applied on MODIS images for the identification of dust sources in the Middle East. Since at that time MODIS DB AOD was only prepared in the resolution of 1°, they disregarded it in their local investigations and tried to propose a new dust detection algorithm called Middle East Dust Index (MEDI). However, later they used 0.1-degree resolution MODIS DB AOD to find dust intensity in local sources identified by MEDI (Moridnejad et al., 2015a).

In the present paper we try to improve the knowledge about the long-term spatiotemporal distribution of West Asian dust storms in three ways: (a) the horizontal extent of dusty areas and its changes are investigated by using a refined threshold of TOMS-OMI AI from 1980 to present, except 1993–1996 and 2002–2004, (b) the MODIS DB AOD is examined from 2003–2014 to determine dust sources by the analysis of dust storm intensity within already identified dusty areas, and (c) The main paths and receptors of dust storms are identified by applying the spatiotemporal lag-correlation method to MODIS DB AOD data. Furthermore, dominant atmospheric patterns which govern the mechanisms of dust relocation are studied. The rest of this paper is organized as follows: methods and data are presented in the next section. The research findings are presented and discussed in Section 3. Section 4 is allotted to conclusions and future work.

2. Data and methods

TOMS-OMI AI is known as the longest aerosol records from 1979 to present. TOMS installed on Nimbus 7 recorded data from 1979 to 1993 with a spatial resolution of 1 × 1.25°. After a 4-year cessation, it continued data gathering on the Earth Probe platform until the end of its operation in 2005. With one-year data overlap, OMI has provided AI in the resolution of 0.25° from 2005 to present. In this study, TOMS-like OMI AI, named OMTO3d_V003, in 1-degree resolution, was used to have a more consistent dataset. The accuracy and precision of the OMTO3d_V003 are similar to the legacy TOMS data, except over cloudy areas where OMTO3d_V003 data is more accurate than that of the TOMS (Ahmad et al., 2004; Vasilkov et al., 2008).

However, the examination of these two datasets shows some uncertainties. As documented in Kiss et al. (2007), the Earth Probe TOMS records are affected by calibration drift issues. The problem (a wavelength dependent calibration drift from changes in the optical properties of the front scan mirror) became worse in 2005 so that the TOMS AI data in the period 2002–2005 are unreliable and cannot be used, especially for any kind of trend analyses.

In addition, area average of long-term daily mean AI over West Asia shows that OMI has steadily recorded lower AI compared to TOMS (Fig. 1). The offset could have climatological reasons but also artificial reasons caused by different instrument characteristics. In fact, it is shown below that the change of instruments caused an artificial decrease in AI which can cause misinterpretation of dust activity in recent years. Such data inhomogeneities are serious

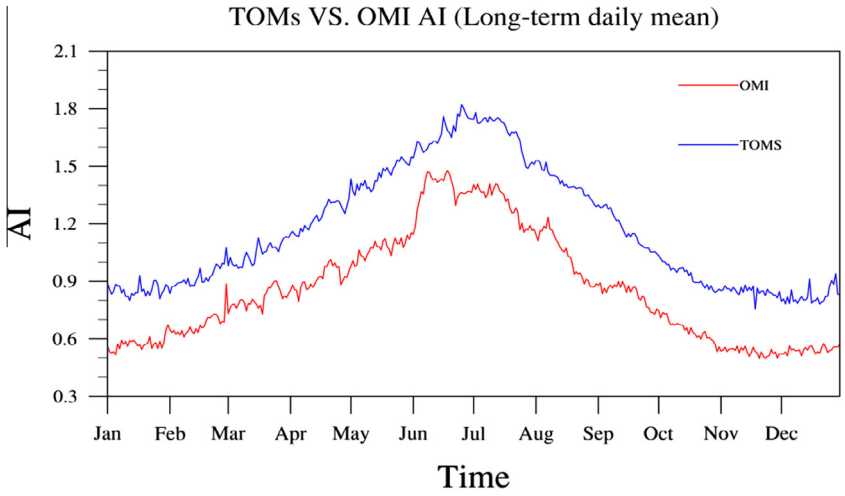

Fig. 1. Area average of long-term daily mean AI over West Asia (20N–40N and 35E–65E). Blue curve shows area-averaged TOMS AI between 1980 and 2001 and red curve represents OMI AI between 2005 and 2014. (For interpretation of the references to colour in this figure legend, the reader is referred to the web version of this article.)

issues in climate science since they can completely mask or even reverse an existing climate change signal. For atmospheric temperature, data homogenization has become a standard procedure before interpreting any data (Mears et al., 2003; Haimberger, 2007; Venema et al., 2012; Haimberger et al., 2012). More and more satellite data are reprocessed in order to reduce the effect of calibration drifts and -offsets between various instruments. In our particular case, we have to offset the different calibration of TOMS and OMI. The lack of temporal overlap period between reliable TOMS data and OMI data makes it particularly challenging to create homogeneous climatological time series derived from AI.

Another, aforementioned, problem is AI sensitivity to dust layer height which caused AI overestimation (underestimation) in warm (cold) periods or areas. As shown in Fig. 2, highlands in western Saudi Arabia host a constant high boundary layer (Dee et al., 2011). This has a profound effect on aerosol height and yields significant biases in the intensity of recorded AI in the region (discussed later). The effect of aerosol height on AI is so obvious that Ginoux and Torres (2003) have taken planetary boundary layer height (h_{PBL}) as one of the main inputs for the simulation of AI.

In order to tackle all above-mentioned issues, following measures are taken:

1. Besides the data gap between 1993 and 1996, AI recorded by TOMS during 2002–2004 are excluded from further examinations.
2. Because of higher accuracy of OMI AI over cloudy pixels, long-term study of AI is limited to warm months (April–September) when subtropical high pressure is dominant atmospheric pattern over West Asia resulting in mostly cloud free conditions throughout the region.
3. Following Mahowald and Dufresne (2004) we do not use directly AI or FT. Instead we have prepared a VT for the warm months to deal with the sensitivity of AI data to aerosol height. Here VT was defined as the multi-year average of AI simultaneous with SeaWifs DB AOD between 0.5 and 0.55 during warm months. It is worth mentioning that choosing this range is based on subjective examinations of SeaWIFS DB AOD during 65 dust storms between 1998 and 2010 and conducted researches by Mahowald and Dufresne (2004) and Moridnejad et al. (2015a). In fact, DB AOD 0.5–0.55 is used to make sure that intense dust cases are excluded from the preparation of VT so that it is only determined by varying boundary layer height and a roughly constant dust concentration.

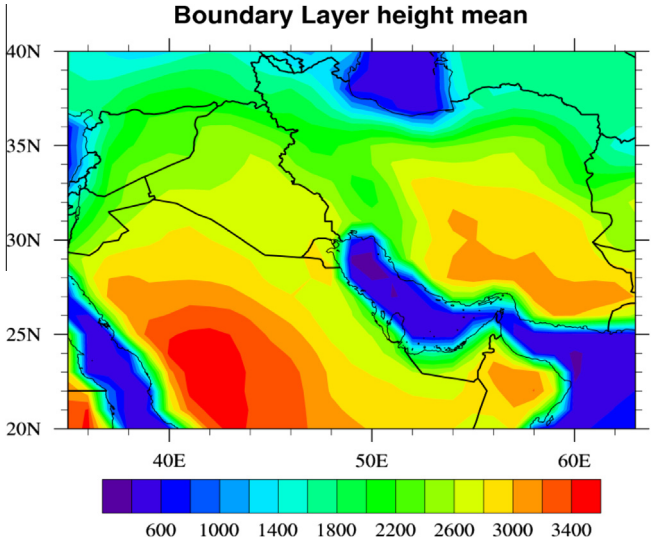

Fig. 2. Long term mean of boundary layer height (m) during the warm season (April–September) 1980–2014 at 12Z from ERA-Interim reanalyses (Dee et al., 2011).

4. Regarding the different distribution of AI measured by TOMS and OMI, VT is separately prepared for these two instruments. To do so, SeaWifs DB AOD between 1998–2001 and 2005–2010 is respectively used for calculating VT of TOMS and OMI. Fig. 3 illustrates the homogenization strategy used for the preparation of AI-based VT.
5. In order to examine efficiency of SeaWIFS DB as an indicator of dust occurrence, it is checked against four AErosol RObotic NETwork (AERONET) stations located in Saudi Arabia and Persian Gulf countries (see Figs. 4 and 7).

Considering different spatial resolution and instrumental characteristics of surface stations compared to satellite data, the agreement of SeaWIFS DB AOD with these stations is acceptable. While the lowest correlation (Null.65) belongs to Dhadnah, it increases orderly in Kuwait (0.68), Solar Village (0.7), and Mezaria (0.81) (Fig. 4A–D). This agreement ensures to a great extent that SeaWIFS DB AOD can detect the outbreak of dust storms and exclude severe dust cases by using threshold 0.5 < AOD < 0.55. Fig. 5 shows separate VTs for TOMS (Fig. 5A) and OMI (Fig. 5B). Over some regions

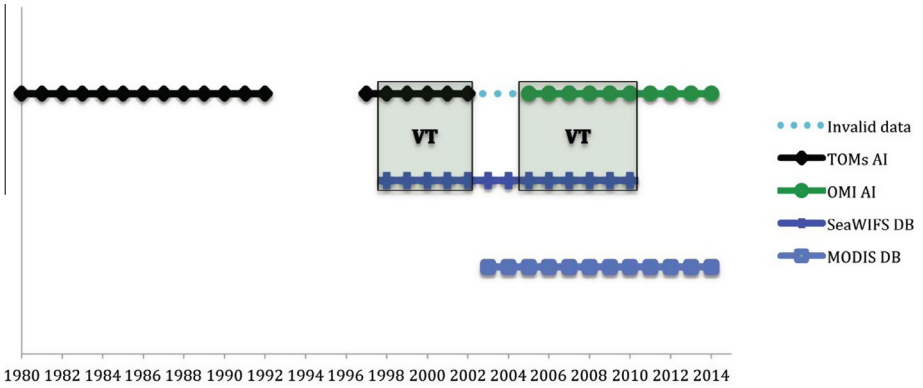

Fig. 3. Timeline of availability of different satellite data used in this study. Systematic differences between TOMS and OMI AI are offset by different varying thresholds used for calculation of FoO from AI. Note SeaWIFS is only data set with significant overlap with both TOMS and OMI. Rectangles indicate time intervals used for calculating the VTs.

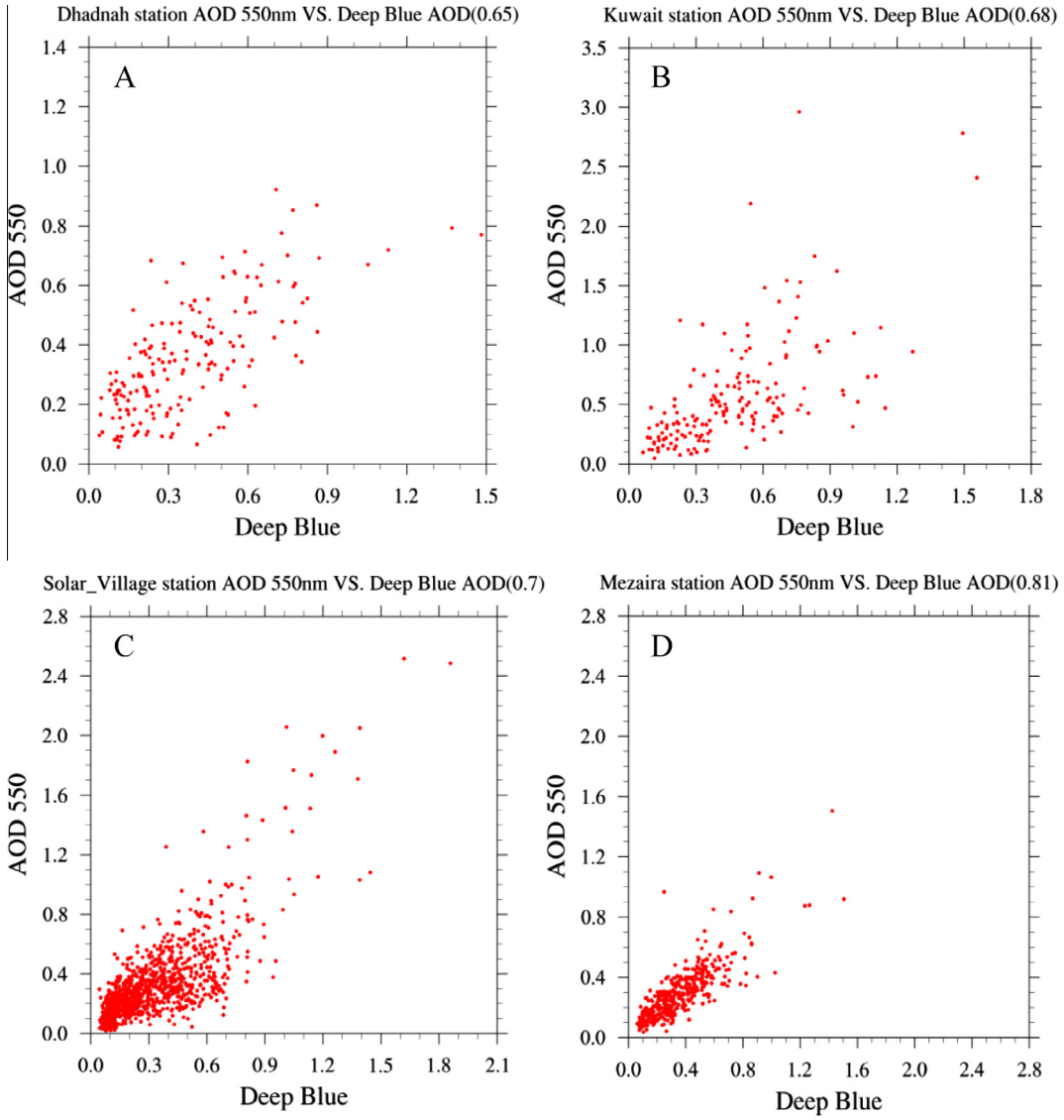

Fig. 4. Scatter plots between SeaWIFS DB AOD 550 nm and AERONET stations AOD 550 nm for stations A) Dhandah (25.5 N and 56.31E), B) Kuwait University (29.31 N and 47.96E), C) Solar Village (24.9 N and 46.38E), and D) Mezaria (23 N and 53.76E), see also Fig. 7. Values in parantheses are Spearman correlation coefficients.

the AOD has never been between the thresholds and therefore there is not complete data coverage in these figures. As discussed earlier, AI is not only function of aerosol concentration, but also it is affected by boundary layer (aerosol) height. Assuming a constant dust concentration by the use of AOD between 0.5 and 0.55, high VT in the west of Saudi Arabia, especially in TOMS VT,

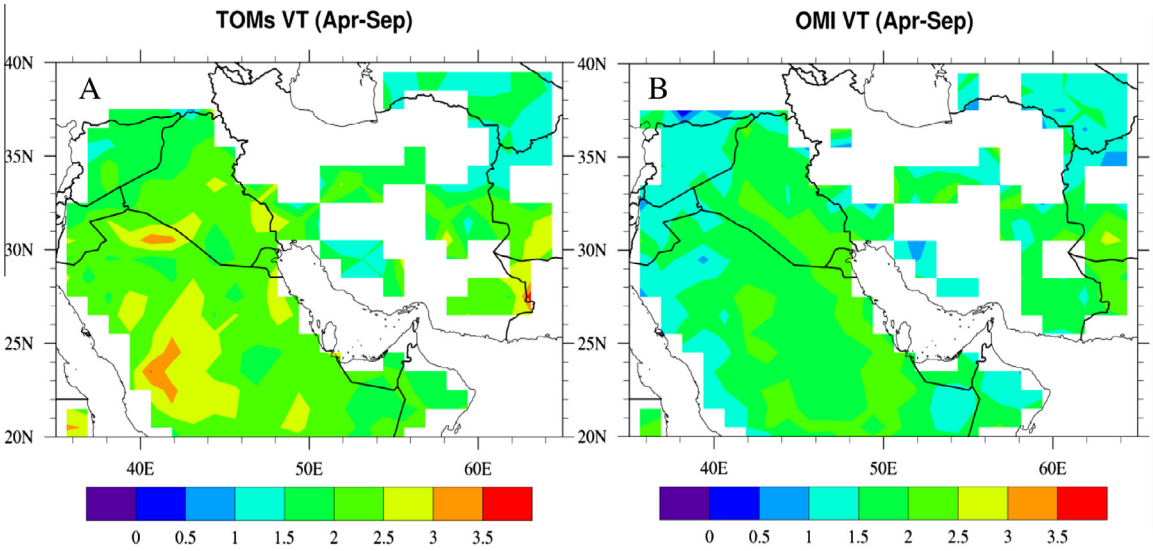

Fig. 5. VT for TOMS AI (A) calculated using SeaWIFS DB AOD for the period 1998–2001 and OMI AI (B) calculating using SeaWIFS DB AOD for period 2005–2008. White areas indicate no data (AOD (almost) never between 0.5 and 0.55).

is because of high boundary layer in the region (Fig. 2). As expected, OMI VT is generally lower than TOMS VT throughout the study region which offsets higher AI recorded by TOMS.

Frequency of Occurrence (FoO) of dust defined as the number of days where AI data exceed a previously defined VT, is used here to measure dust activity changes over time. Therefore the consistency of VTs over TOMS and OMI periods is critical. The VT consistency is tested by the ratio of the multi-year monthly sum of Frequency of Occurrence (FoO) of dust storms detected by VT throughout West Asia to corresponding cases determined by SeaWIFS DB AOD > 0.5. This ratio is separately made for TOMS and OMI by the comparison AI and DB in two periods 1998–2001 and 2005–2008, respectively. To make a comparison, the same process is done for FT, AI > 1 Prospero et al. (2002), shown in Fig. 6.

Although TOMS and OMI VT are a yielding higher number of dust cases compared to DB (between 4 and 6 times), they resulted in an approximately same ratio in both periods. This consistent ratio is a necessary condition that determined changes by AI are caused by real changes in dust frequency and are not significantly affected by the use of different instruments. The higher ratio of FoO for OMI VT compared to TOMS VT in August and September means that there might be a slight underestimation of TOMS VT FoO in these months. We also note that this homogenization procedure depends on the homogeneity of SeaWIFS data. So far we have not found any indications that the SeaWIFS data are inhomogeneous.

In contrast, FT FoO ratios are obviously different during TOMS and OMI periods. This is because of temporal discontinuity of AI due to instrumentation changes. While the ratio of TOMS FT FoO to DB FoO varies profoundly from 10 to 30, it is much lower and more stable in OMI period. This leads to an artificial decrease in the number of detected dust cases by OMI FT in recent years which will be discussed later.

In addition to the examination above, the performance of FT and VT is also evaluated by using a contingency table in the next section. In this method, the variable "*a*" represents true positives, the number of dust events detected by DB AOD (AOD > 0.5), FT (AI > 1) and VT; the variable "*b*" represents false positives, the number of times where DB indicates "no dust," but FT and VT indicate "dust"; the variable "*c*" represents false negatives, the number of times where DB indicates "dust," but FT and VT indicate "no dust"; the variable "*d*" represents true negatives, the number of times where all three algorithms indicate "no dust". These four elements are components of accuracy equation:

$$\text{Accuracy}(\%) = \frac{a+d}{a+b+c+d} * 100 \quad (3)$$

Having done verification, dusty areas of West Asia were identified through annual analysis of VT FoO. As the study period was divided into two 14-year periods: 1980–1997 (with a 4-year data gap) and 1998–2014 (with a 3-year data gap). The VT FoO of 800 and 500 days per each 14 years were used, as two empirical thresholds, to separate permanent, extinct and emerging dusty areas. Permanent dusty were defined as where have a FoO > 800 in both periods 1980–1997 and 1998–2014. Emerging areas have FoO < 500 in 1980–1997 and FoO > 500 in 1998–2014 in most pixels. Extinct areas (practically nonexistent) have FoO > 800 in 1980–1997 and FoO < 500 in 1998–2014. In order to discriminate dust sources from affected regions in identified dusty areas, the intensity of dust emission is locally examined by the use of MODIS DB AOD which is accessible from 2003 to present. In this study, total FoO of MODIS DB AOD > 0.85 during warm months is considered as the indicator of dust sources (Moridnejad et al., 2015a). After determination of dust sources, main dust paths and receptors were identified by the use of lagged cross-correlation between MODIS DB AOD of dust sources and the whole region (Ke-Yi, 2010).

Besides using remotely sensed data, meteorological stations data are also used in some parts of study to validate results. These data are acquired from synoptic stations in western Iran (Fig. 7). In the following image, synoptic stations in the southwest of Iran (Khuzestan plain) are discriminated with a red background which will be discussed in the next section. Furthermore, AEORONET stations used earlier for the validation of SeaWIFS DB are shown by stars.

3. Results and discussion

In order to describe the long-term behavior of dust storms in West Asia, FT FoO and VT FoO of dust storms, during warm months, are summed up in seven 4-year time slices from 1980 to 2014 (Fig. 8). It is worth to mention that time slices between 1992–1999 and 2000–2006 have 4 and 3-year data gaps, respectively.

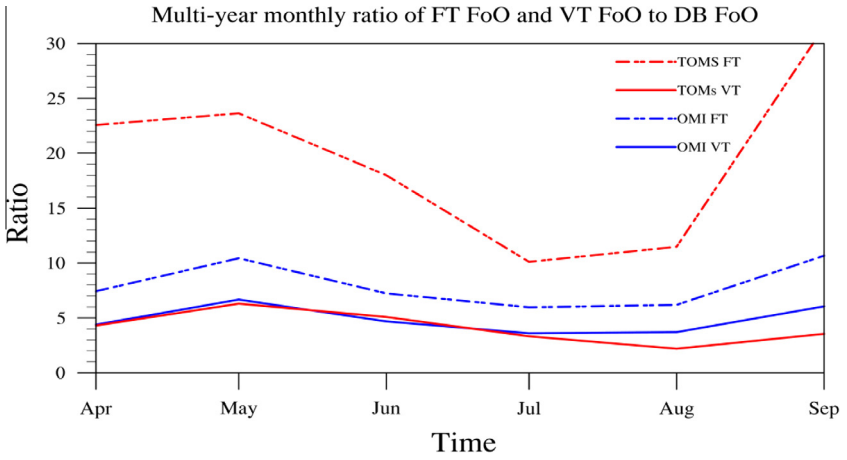

Fig. 6. Multi-year monthly ratio of FoO of dust storms determined by FT and VT to FoO detected by SeaWIFS DB AOD for the periods 1998–2001 (TOMS) and 2005–2008 (OMI).

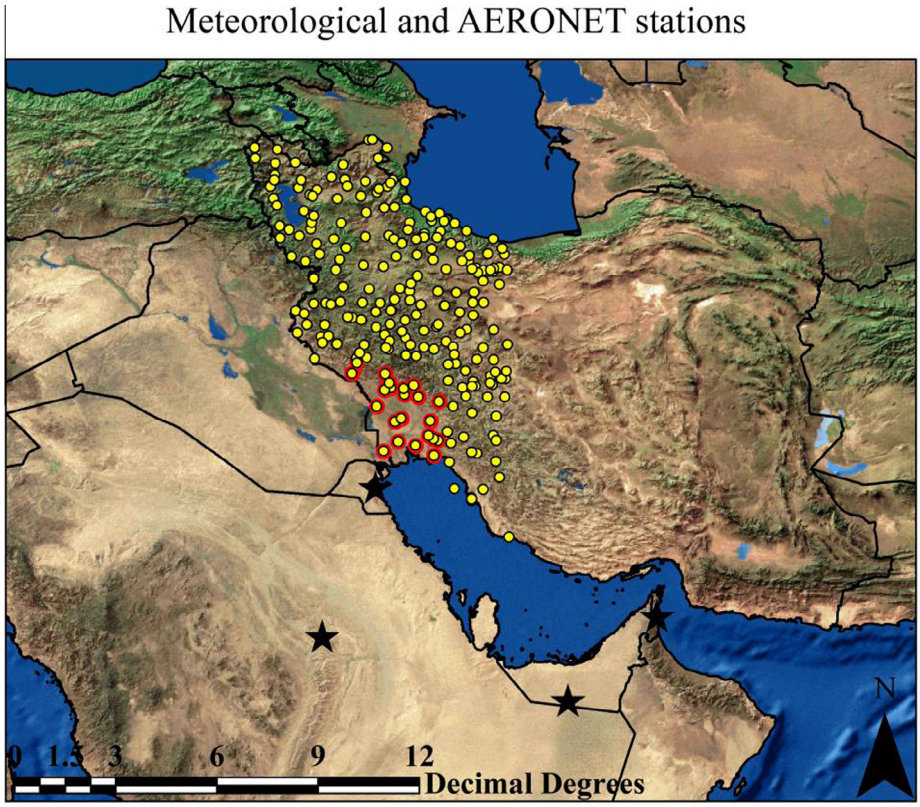

Fig. 7. Synoptic stations in the western half of Iran (yellow dots). Yellow dots with red background are stations in Khuzestan plain. Stars indicate the location of AERONET stations used for comparison with SeaWIFS DB AOD. (For interpretation of the references to color in this figure legend, the reader is referred to the web version of this article.)

Apart from the constant overestimation of FT FoO to VT FoO, the most obvious difference between them is the reverse trend of dust activity after 2006. As discussed in the last section (Fig. 6), the number of detected dust storms (FoO) by FT is much lower in OMI period which is because of the general reduction of AI recorded by this instrument (Fig. 1). For example, the Rub al Khali desert[3], in the east of Saudi Arabian Peninsula, is shown by a lower number dust cases between 2011 and 2014 comparing to 2000–2006. This is while VT yields the same or even higher number of cases in the 2011–2014 period. Another instance is northwest of Iraq where VT FoO increases between 2007 and 2010. However, corresponding FT FoO shows a decrease during the same period. In fact, the use of OMI FT caused a reduction of detected dust cases between 2007 and 2014[4]. In addition to instrumental discontinuity, the offensive effect of boundary layer height on AI is remarkably seen among FT FoO, especially during TOMS period, in the western half of Saudi Arabia and southeast of Iran. According to total difference between FT FoO and VT FoO (Fig. 9A), these overestimations occur mostly in regions where boundary layer height is correlated with AI

[3] The empty quarter.

[4] Although OMI FT is also involved in time slice of 2000–2006, because two years of that (2000 and 2001) are TOMS AI, the significant reduction is seen after this period.

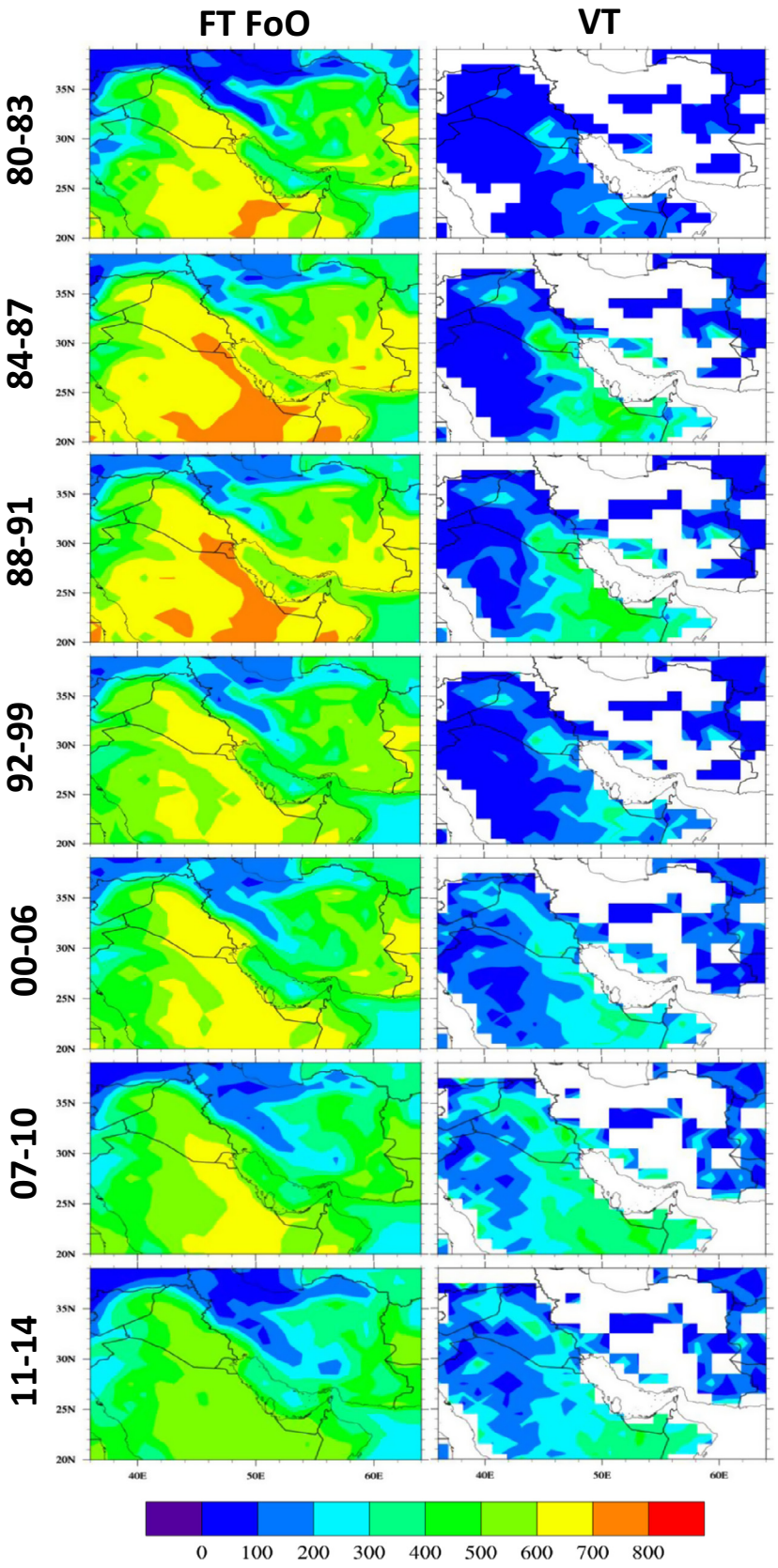

Fig. 8. 4-year FoOs in units days of dust storms in West Asia based on FT (left) and VT (right) for time different intervals (1980–1983, 1984–1987, . . .) in the period 1980–2014. Intervals 1992–1999 and 2000–2006 appear longer but contain only 4 years of valid data as well.

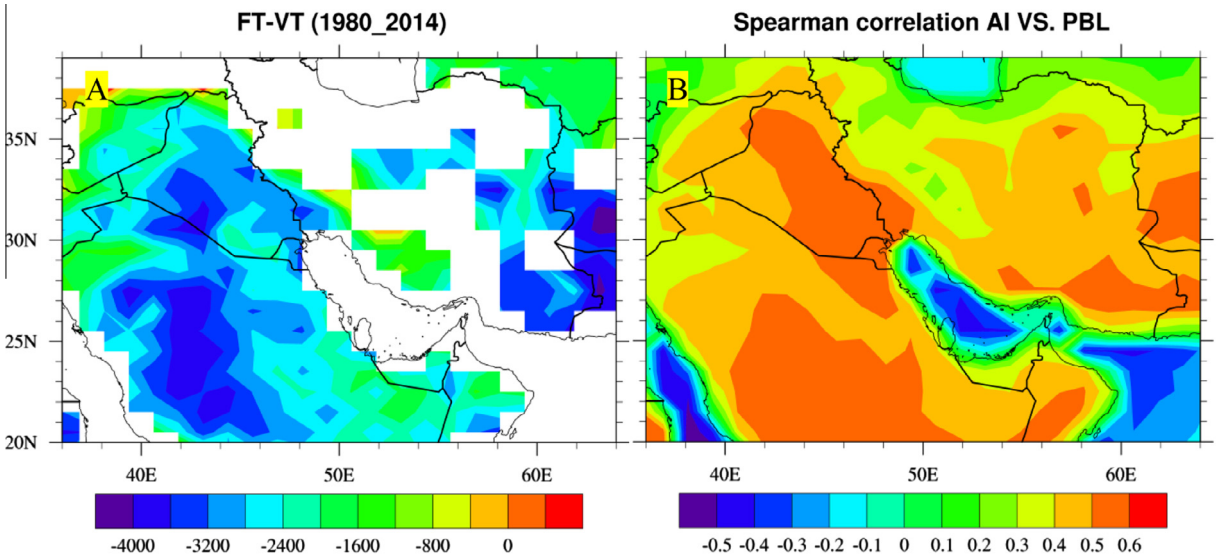

Fig. 9. Panel A: Overall difference between FT FoO and VT FoO in units days from April to September for the period 1980–2014. Panel B: Spearman correlation coefficient between AI and Planetary Boundary Layer (PBL) height during April to September from 1980 to 2014.

(Fig. 9B). In fact, positive correlations represent desert areas where high boundary layer height can be assumed as the main reason of AI overestimation.

The accuracy (Eq. (1)) of FT and VT is evaluated based on both SeaWIFS DB and MODIS DB products. Concerning that VT is prepared by using SeaWIFS DB, it is better not to use it also for the verification. However, the main barrier is that MODIS DB does not cover any part of TOMS period. So verification is first done by the use of SeaWIFS DB for both TOMS (1998–2001) and OMI periods (2004–2010) and then OMI (2005–2014) is also verified by MODIS DB. In this way, we can compare OMI verifications based on both instruments and make sure that the reliance of VT on SeaWIFS DB cannot mislead. The accuracy of TOMS (Fig. 10A) and OMI (Fig. 10B) FT against SeaWIFS DB shows a similar pattern namely the lowest accuracy in the west of Saudi Arabia, south of Iraq and southeast of Iran. These are regions where VT could bear a significant improvement for both instruments (Fig. 10D and E). Although the accuracy of OMI FT rises when MODIS DB is used (Fig. 10C), it also causes higher accuracy for OMI VT (Fig. 10F). Regarding the similar pattern of TOMS and OMI accuracy using both SeaWIFS and MODIS DB and higher accuracy of VT, it can be concluded that VT is much more reliable than FT for the detection of dust storms during the whole study period.

As explained in Section 2, we have used VT-based FoO to separate permanent (Fig. 11A), emerging (Fig. 11C) and extinct dusty areas in the region. The permanent dusty areas are mostly identified in the east of Saudi Arabia. Based on annual area-averaged VT FoO, after two main upsurges of permanent dusty areas in 1984 and 1991, the most recent peak happened in 2008 in this region (Fig. 11B). The sample average and standard deviation of the mean of permanent dust areas have changed from 73 and 8.5 during 1980–1992 to 75 and 6.8 during 1997–2014. The annual area-averaged FoO of dust storms of emerging dusty areas, covered the east of Syria, northwest of Iraq, and a small area in the Sistan Basin in eastern Iran, has strongly increased in recent years, with a peak in 2008. Similarly, dust frequency average and standard deviation of the mean of emerging areas have profoundly increased from 22 and 3.9 to 67 and 7.8, respectively (Fig. 11D). This implies more frequent and fluctuating dust events in emerging dusty areas during the past decade. It is worth mentioning that episodes of low/high dust frequency in emerging areas have coincided with permanent areas. This can be attributed to the fact that dust factors, like drought, or/and the resulting dust plumes affect most of the region during dusty periods. As an example, Trigo et al. (2010) studied a very intense drought in Fertile Crescent[5] between 2007 and 2009 found as the driest two-year case for the region since 1940.

This drought has taken place exactly when emerging and, with less frequency, permanent areas have been simultaneously activated. Fig. 12 shows that most parts of dusty areas, especially emerging ones, were under a very profound reduction of precipitation during October–May in 2007–2008 (Fig. 12A) and 2008–2009 (Fig. 12B).

Interestingly, Notaro et al. (2015) have found that the upsurge of dust storms in Saudi Arabia between 2008 and 2012 mostly originated from drought-stricken sources across the Fertile Crescent. In fact, it can be inferred that while dust intensification of emerging dusty areas is mostly because of local intense drought, permanent dusty areas are affected by local drought-driven dust cases and intensified dust storms in Iraq traveling to Arabian Peninsula. It is worth mentioning that extinct areas, i.e. to be active only in the first period, were also considered, but very few points with decreasing dust frequency were found in the recent period (not shown here). This means that dust sources of West Asia have been mostly growing in three last decades.

Fig. 13 shows the area-averaged monthly VT FoO in permanent (13-A) and emerging (13-B) dusty areas during last decades, except 1993–1997 and 2002–2004. In the permanent dusty areas, dust storms spread in all warm months with a peak in June and July during the whole study period. Conversely, the monthly distribution of dust storms in emerging areas shows two different periods of dust activity from 1980 to 2000 and after that. In the first period, there were only few dust cases mainly in July. In the second period, the number of dust cases increased markedly and the period of dust activity expanded to whole warm months. This affirms that dust frequency has increased both spatially (Fig. 11C) and temporally (Fig. 13B) in the emerging dusty areas.

[5] The Fertile Crescent is the region in the Middle East which curves, like a quarter-moon shape, from the Persian Gulf, through modern-day southern Iraq, Syria, Lebanon, Jordan, Israel and northern Egypt.

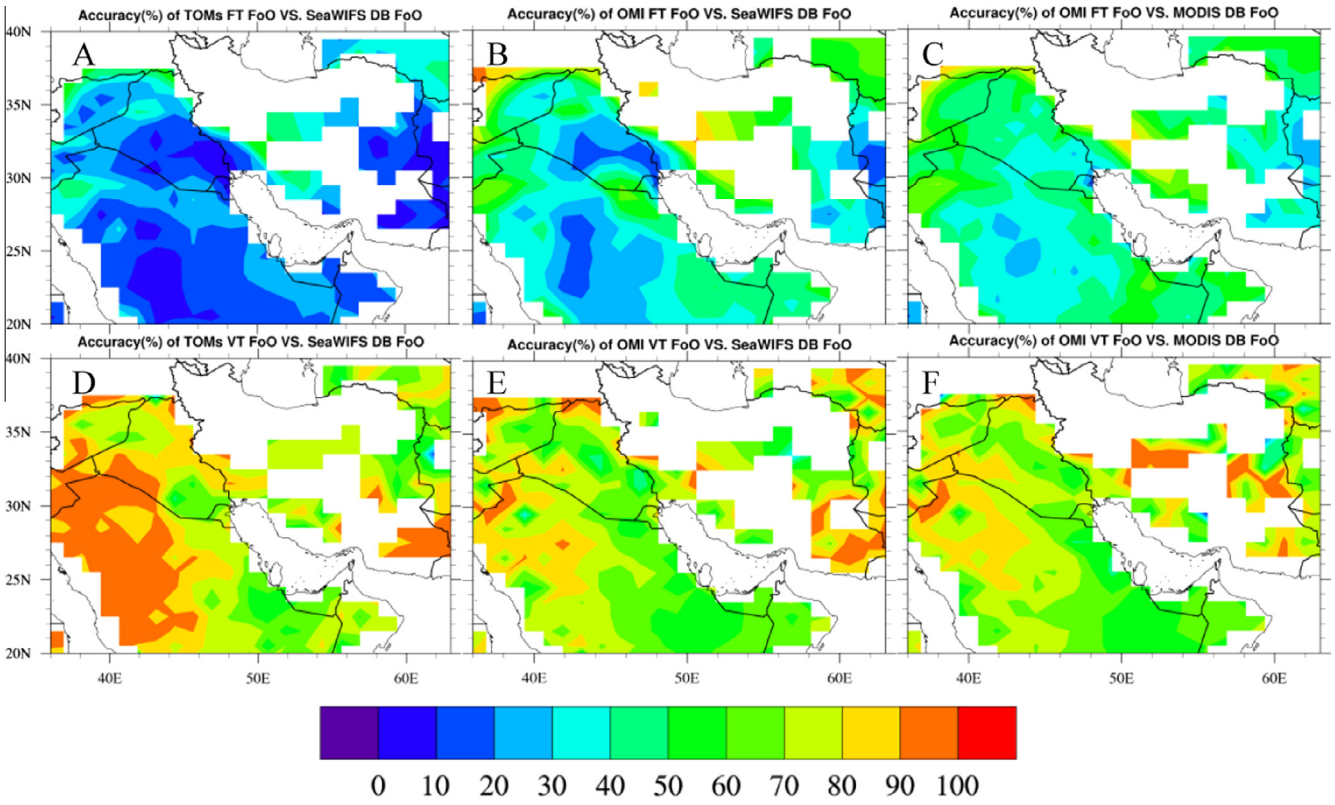

Fig. 10. Accuracy (%) of TOMS FT against SeaWIFS DB (A), OMI FT against SeaWIFS DB (B), OMI FT against MODIS DB (C), TOMS VT against SeaWIFS DB (D), OMI VT against SeaWIFS DB (E), and OMI VT against MODIS DB (F). Missing pixels in FT figures are advertently made to have an appearance like VT.

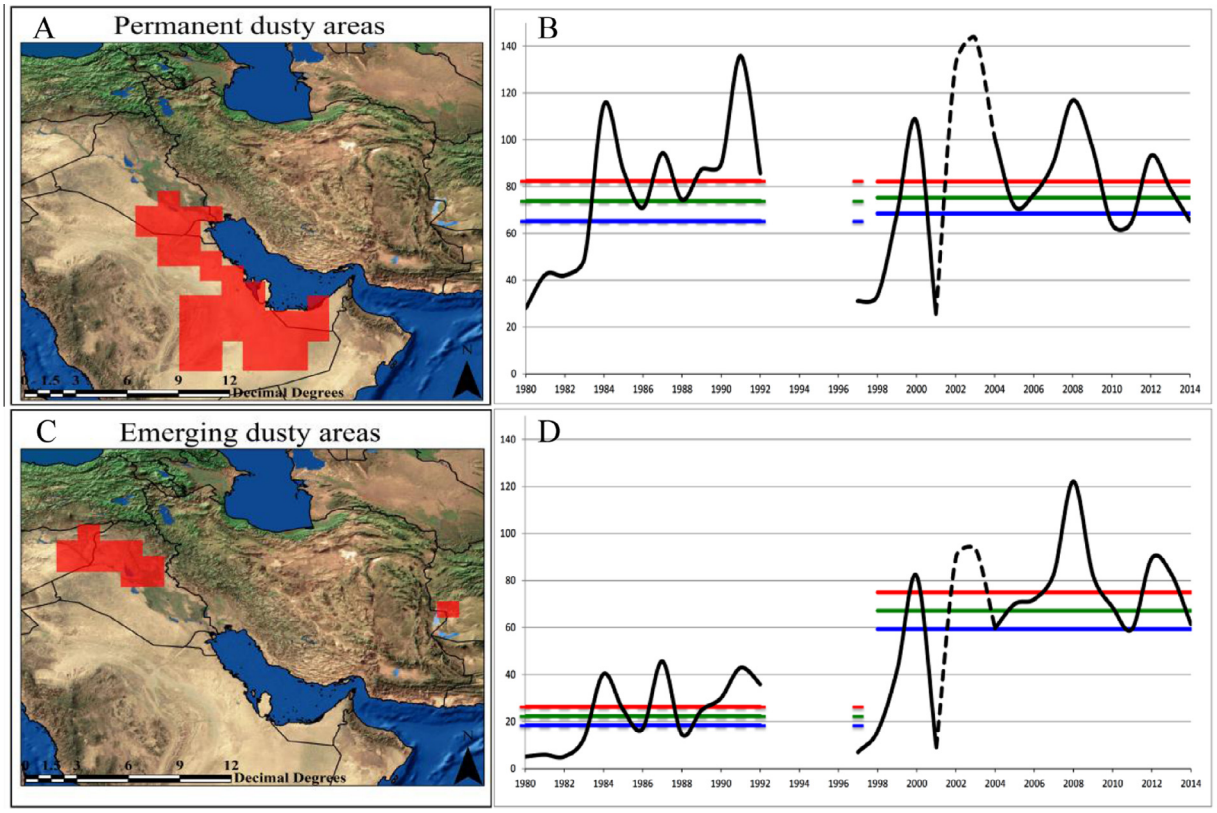

Fig. 11. Permanent (A) and emerging (B) dusty areas in West Asia from 1980–2014. C and D are respectively the area-averaged annual FoOs of VT-detected dust storms within permanent and emerging dusty areas. The blank belongs to data gaps between 1993 and 1997 and dash line is the representative of invalid data between 2002 and 2004.

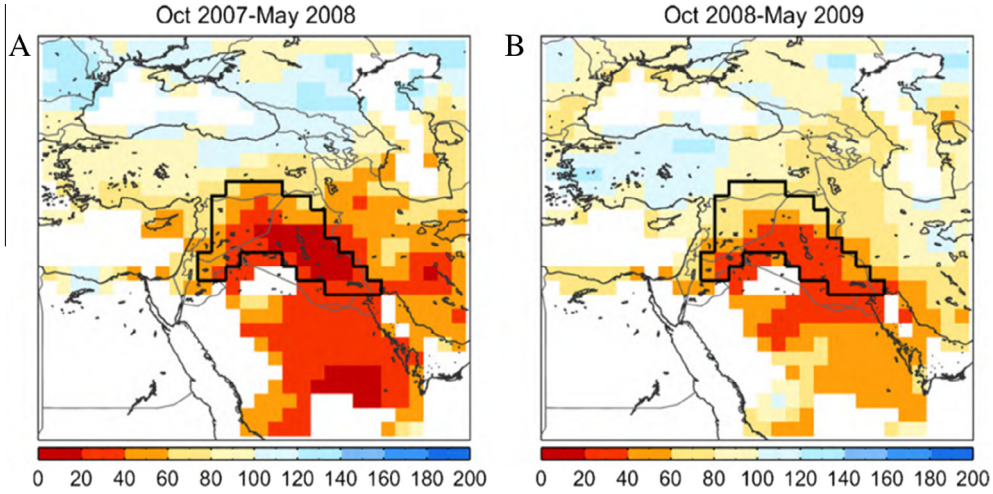

Fig. 12. Accumulated monthly precipitations (expressed in percentage relative to the 1940–2009 normal) during October to May in 2007–2008 (a) and 2008–2009 (b). Black polygon is the boundary of Fertile Crescent (Trigo et al., 2010).

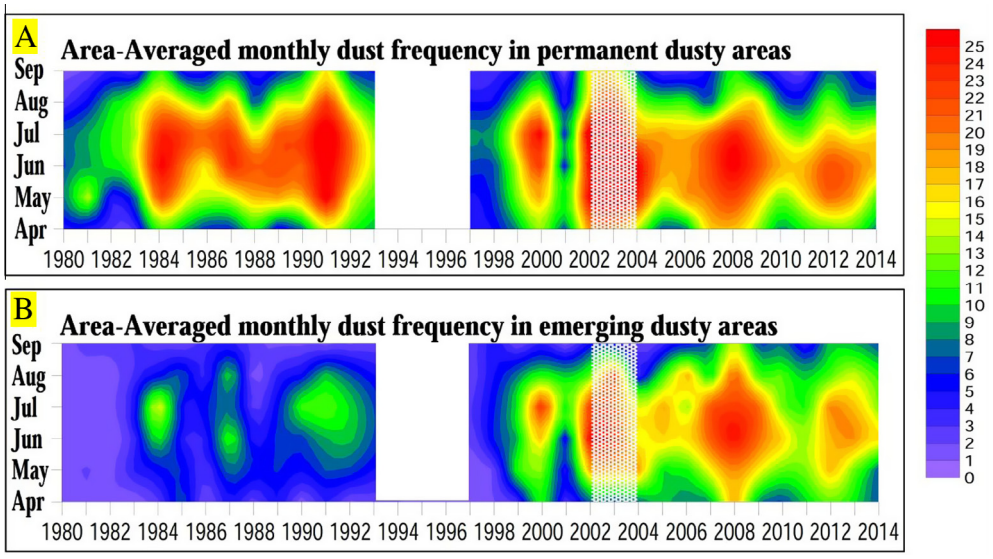

Fig. 13. Area averaged monthly VT FoO (averaged number of dusty days per month) in A) permanent and B) emerging dusty areas as indicated in Fig. 11. Data gap 1993–1997 and invalid data 2002–2004 are masked and blurred, respectively.

In order to validate these results and to check if monthly dust distribution is properly represented on dusty areas by VT, these examinations are also done for southwestern Iran. This region has been chosen since its weather data are freely available from 1980 to present and since it is frequently hit by dust storms coming from the western half of the region (discussed later). The most reliable meteorological data related to dust storms are weather codes. For this study, all meteorological dust codes, 6–9 and 30–35 (WMO, 2011), acquired from synoptic stations in Khuzestan plain are considered to have both local and regional dust storms. The comparison of VT-based time series (Fig. 14A) and ground-based observations (Fig. 14B) shows that this refined threshold managed to represent main characteristics of observational time series. For example, the dusty episodes in 1984, 1991, 2000, and 2008 are seen in both distributions. Furthermore, monthly peaks of both time series happened during June to August. Further examinations show that differences between these two time series, such as higher number of cases before 1984 or peak displacement from 2008 in VT FoO to 2009 in observations, can be attributed to the rough resolution of AI which cannot detect local dust cases recorded by meteorological stations.

As discussed earlier, a dusty area consists of both dust emitting and affected spots. To discriminate these regions, those parts of dusty areas that emit high-intensity dust storms are determined as dust sources. Intense dust cases from MODIS DB AOD (Ginoux et al., 2012; Moridnejad et al., 2015a) were defined by FoO of MODIS DB AOD exceeding 0.85.

The tally of intense dust storms covers up main sources of permanent dusty areas spread out in the southeast, east and northeast of Saudi Arabian Peninsula and southeast of Iraq (Fig. 15A). However, most dust sources have been concentrated in the northern part of permanent dusty areas. The examination of the FoO of intense dust storms within emerging dusty areas showed a hot spot in the northwest of Iraq (Fig. 15B). In fact, it can be claimed that northwest of Iraq close to the confluence of Tigris and Euphrates is the main source of recent dust storms in West Asia. In order to find main dust paths and affected areas of these two dust sources, i.e. the northeast of Saudi Arabia and southeast of

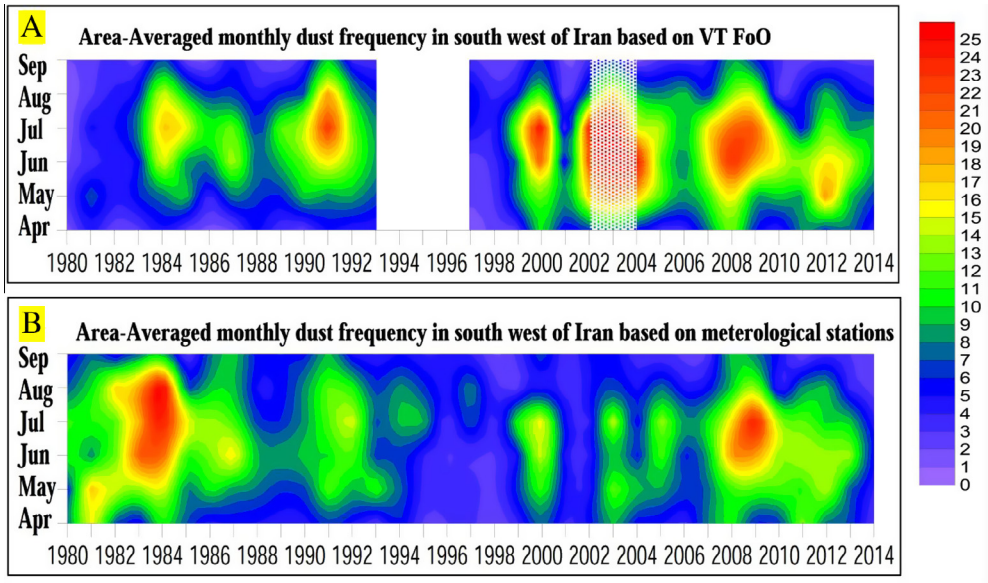

Fig. 14. (A) Area averaged monthly VT FoO (averaged number of dusty days per month) in the south west of Iran based on AI VT and (B) meteorological stations. Data gap 1993–1997 and invalid data 2002–2004 are masked and blurred in figure A, respectively.

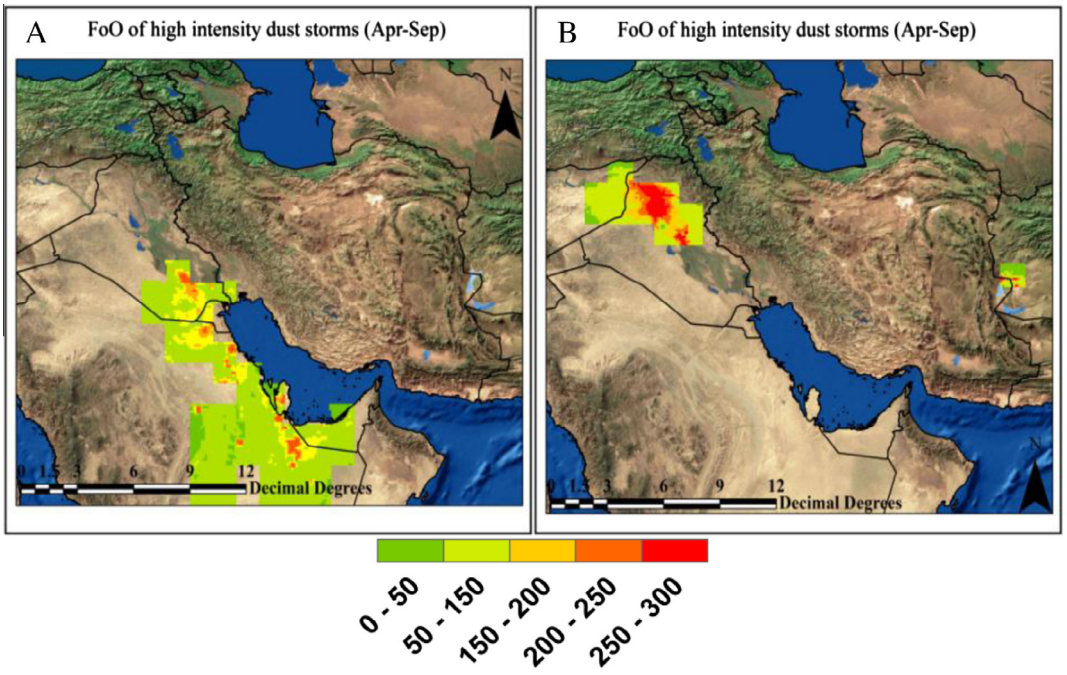

Fig. 15. FoO of high intensity dust storms (MODIS DB AOD > 0.85) in units days during April to September for the whole MODIS period 2003 to 2014 within permanent (A) and emerging (B) dusty areas.

Iraq and northwest of Iraq, a lagged correlation was computed between area-averaged MODIS DB AOD recorded in dust sources and West Asia for warm seasons (Fig. 16). The zero-lagged correlation represents the first day of dust outbreak, it shows the highest correlation with already identified dust sources and their surrounding areas, as expected. This is why zero-lagged correlation of permanent dust sources, during spring, increases getting closer to the southeast of Iraq and northern Arabian Peninsula. However, there is a high correlation tongue toward the north of Iraq and northwest Iran at lag zero (Fig. 16A). At lag 1, there are two moderate correlation clouds to the middle of Iran and south of Saudi Arabia (Fig. 16B).

The extension of a high correlation area to the north of Iraq, northwest of Iran, and south of Turkey is also visible for emerging dust sources, especially at 1-lagged correlation, during March to May (Fig. 16C and D). Since these areas are mountainous and cannot be affected by local dust sources, this pattern means that north of Iraq and northwest of Iran are two of the main receptors of dust storms formed in both dust source areas during spring. During summer, the high correlation of permanent dust sources and study areas is located from the northwest of Iraq to southeast of the east of Saudi Arabia at lag zero (Fig. 16E) and southeast Saudi Arabia and southwest of Iran at lag one (Fig. 16F). Similarly, lagged correlation of emerging dust source and West Asia show a

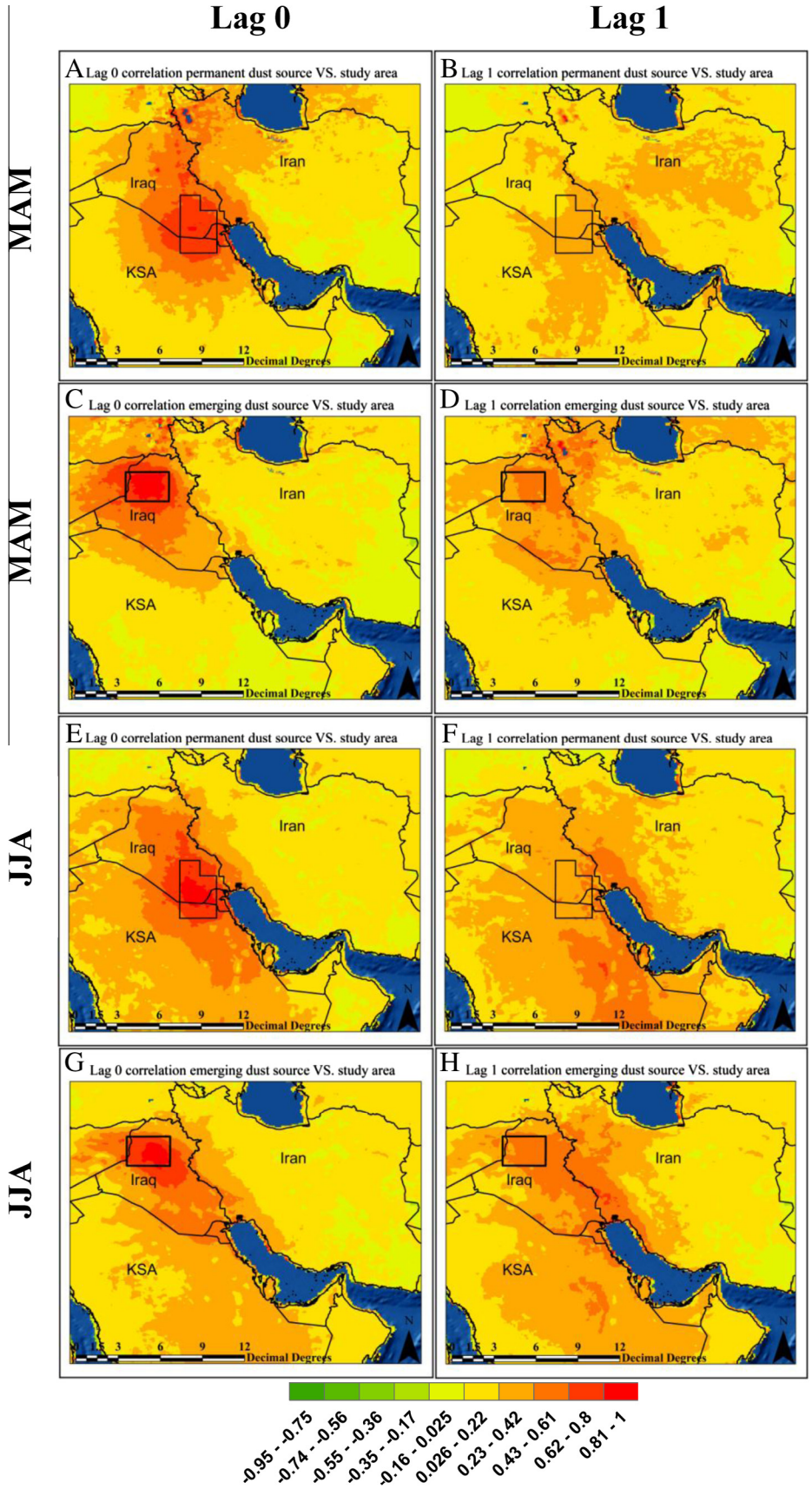

Fig. 16. Map of lagged Pearson correlation coefficients between dust sources, shown by black polygons, and study area during spring (MAM) and summer (JJA), calculated from MODIS DB AOD for period 2003–2014.

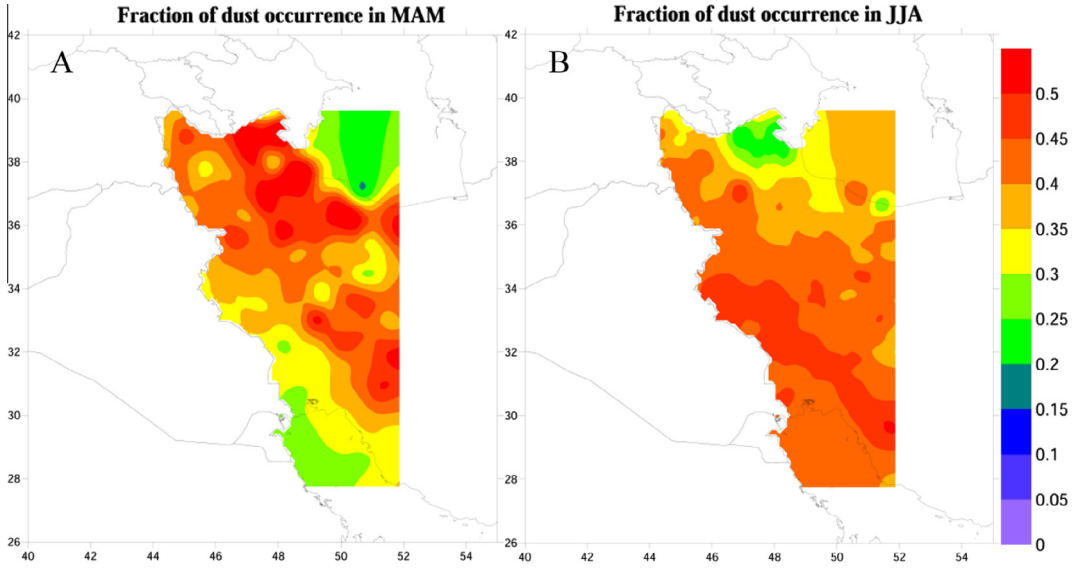

Fig. 17. The fraction of seasonal FoO of dust storms to total annual FoO of dust storms reported by synoptic stations in the West Iran (A) in Spring (B) in Summer for period 1980–2014.

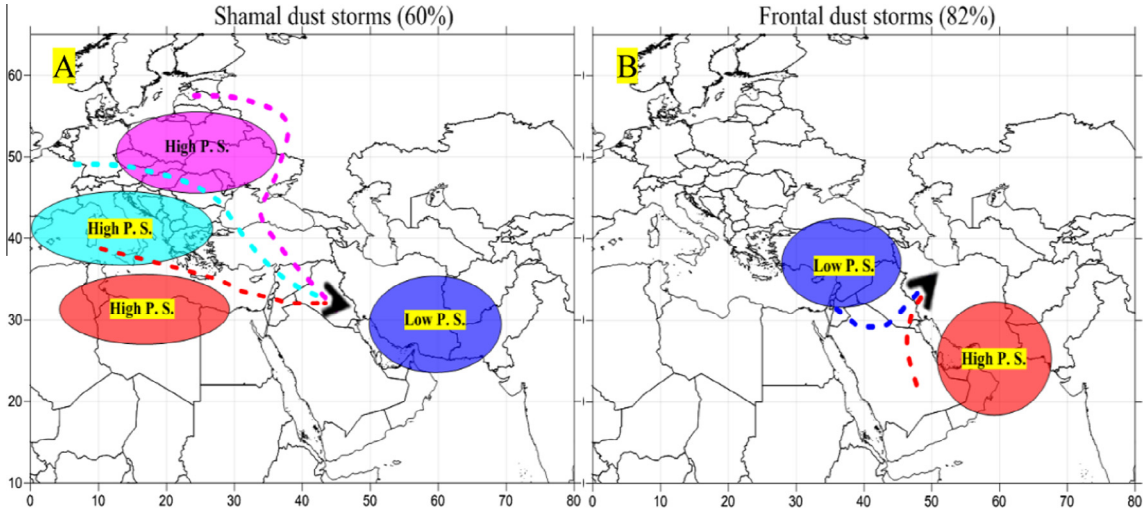

Fig. 18. Atmospheric patterns simultaneous with 60 percent of Shamal dust storms (A) and 86 percent of Frontal dust storms (B) adapted from Hamidi et al. (2013). Colored ellipses and curves are surface pressure systems and blowing winds, respectively. Shamal dust storms may be further classified depending on location of high-pressure systems (East-Central Europe, Mediterranean Sea or North of Africa). (For interpretation of the references to color in this figure legend, the reader is referred to the web version of this article.)

northwest-southeast path from northwest of Iraq to the southwest of Iran (Fig. 16G and H). Although lag-1 correlations of 0.23–0.42 cover most of the region during summertime, this grade of correlation over the Zagros Mountains can be a sign of dust transport from permanent and emerging dust sources to the west and northwest of Iran by thin dust plumes. To sum up, lagged correlation of identified permanent and emerging dust sources show two seasonal distinctive dust paths and receptors. Springtime dust (correlation) paths are both northward and reach south of Turkey and northwest Iran. During summer, dust storms take the northwest-southeast path and affect southwest of Iran, southeast of Iraq, Saudi Arabia, and other Persian Gulf countries. With the intention of verifying identified receptors, because of data accessibility, the seasonal fraction of dust events is examined in the west of Iran, by using meteorological dust codes of synoptic stations (Fig. 7).

Regarding that only dust cases formed in the warm period are studied here, fraction of dust occurrence, i.e. total seasonal FoO of dust storms/total annual FoO of dust storms, is just examined for spring and summer from 1980 to 2014.

According to lag correlation method, northwest and southwest of Iran are two of main receptors of dust storms during spring and summertime, respectively. These patterns are replicated in the 35-year climatologies of seasonal dust fraction. The north and northwest of Iran received the majority (more than 40–50 percent) of annual recorded dust events during spring (Fig. 17A). During summertime, the largest fraction of detected dust storms relocates to the southwest of Iran and it decreases to less than 40 percent in the northwest of this country (Fig. 17B). These patterns are consistent with Hamidi et al. (2013), who identify two main types of dust storms, called Shamal and Frontal dust storms, in West Asia. Analyzing atmospheric circulations of 180 dusty days, they found that Shamal is the most frequent type of dust storms in West Asia. Further examinations showed that 60% of Shamal dust storms are simultaneous with high-pressure systems, to the west of the

region, reaching from northern Europe to north of Africa and a low-pressure system centered over southern Iran. This atmospheric pattern causes strong winds (color dash lines), called Shamal Winds (Strachan, 2005), from northwest of Iraq to Persian Gulf countries (Fig. 18A). This circulation has the highest frequency in June and July when dust storms are mostly recorded in the southwest of Iran (Fig. 17B). During spring, Shamal dust storms are much less frequent but there are frequent dust storms of Frontal type, with high pressure over southern Iran and low pressure over the eastern Mediterranean Sea, Turkey and northern Iraq (Fig. 18B). This kind of circulation, which included 82% of studied Frontal cases transports dust plumes to north and northwest of Iran.

4. Conclusion and future work

This study aimed to investigate long-term activity of dust storms in West Asia, a region which experienced intensified dust storms in recent years. Preparing a Varying Threshold (VT) for Aerosol Index of TOMS and OMI, analysis of dust activity showed a temporal and spatial expansion of dust storms in the east of Syria and northwest of Iraq, called emerging dusty areas, in the last decade. Besides that, east and northeast of Saudi Arabia were found as permanent dusty area emitting large amounts of dust, at least from 1980 onward. The increase of dust storms in West Asia, especially in emerging areas, was attributed to an extreme drought in the Fertile Crescent during 2007–2012. According to monthly distribution of dust storms, June and July are the main periods of dust activity in West Asia. During recent years, dust storms of emerging dusty areas are becoming expanded to the whole warm period of the year what is commonplace in permanent dust areas from the beginning of study period. In order to discriminate dust sources from affected areas which constitute dusty areas, high-intensity dust storms are examined as an indicator of dust sources. Results show two main dust sources in the northwest of Iraq and southeast of Iraq and northern Saudi Arabia. Subsequently, the lagged correlation method revealed that there two distinct dust paths and receptors during spring and summertime in West Asia. During spring, dust storms are transported to the north of Iraq and northwest of Iran by a Frontal mechanism. During summer, Shamal atmospheric pattern makes dust plumes take northwest-southeast direction hitting southwest of Iran and Persian Gulf countries.

Considering the fact that the comprehensive understanding of dust storm is not achievable only through the study of its horizontal distribution, the future work aims to investigate the vertical structure of this phenomenon in West Asia. This can be done by using Weather Research and Forecasting model coupled with Chemistry (WRF-chem, (Grell et al., 2005)) simulations and Cloud-Aerosol Lidar and Infrared Pathfinder Satellite Observations (CALIPSO, (Ma et al., 2013; Adams et al., 2012)) products but is beyond the scope of this paper.

Acknowledgements

This work has been financially supported by EU 7th framework program ERA-CLIM (No. 265229) and the Austrian Science Funds FWF (Project P25260-N29).

References

Ackerman, S.A., 1989. Using the radiative temperature difference at 3.7 and 11 μm to tract dust outbreaks. Remote Sens. Environ. 27, 129–133.
Adams, A.M., Prospero, J.M., Zhang, C., 2012. CALIPSO-derived three-dimensional structure of aerosol over the Atlantic Basin and adjacent continents. J. Clim. 25, 6862–6879.
Ahmad, Z., Bhartia, P., Krotkov, N., 2004. Spectral properties of backscattered UV radiation in cloudy atmospheres. J. Geophys. Res. Atmos. 109.
Ahmad, S.P., Torres, O., Bhartia, P., Leptoukh, G., Kempler, S., 2006. Aerosol index from TOMS and OMI measurements. In: Proc. of the 86th AMS Annual Meeting.
Al Sarraf, H., 2010. Relationship between the land/sea breeze circulations and the air pollution dispersion over the coastal area of Kuwait.
Aurelius, L., Buttgereit, V., Cammelli, S., Zanina, M., 2007. The impact of Shamal winds on tall building design in the Gulf Region. Proceedings.
Azizi, G., Shamsipour, A., Miri, M., Safarrad, T., 2012. Synoptic and remote sensing analysis of dust events in southwestern Iran. Nat. Hazards 64, 1625–1638.
Boloorani, A.D., Nabavi, S.O., Bahrami, H.A., Mirzapour, F., Kavosi, M., Abasi, E., Azizi, R., 2014. Investigation of dust storms entering Western Iran using remotely sensed data and synoptic analysis. J. Environ. Health Sci. Eng. 12, 124.
Cao, H., Amiraslani, F., Liu, J., Zhou, N., 2015. Identification of dust storm source areas in West Asia using multiple environmental datasets. Sci. Total Environ. 502, 224–235.
Ciren, P., Kondragunta, S., 2014. Dust aerosol index (DAI) algorithm for MODIS. J. Geophys. Res.: Atmos. 119, 4770–4792.
Dee, D., Uppala, S., Simmons, A., Berrisford, P., Poli, P., Kobayashi, S., Andrae, U., Balmaseda, M., Balsamo, G., Bauer, P., 2011. The ERA-Interim reanalysis: Configuration and performance of the data assimilation system. Quartly J. R. Meteorol. Soc. 137, 553–597.
Ebrahimi, S.J., Ebrahimzadeh, L., Eslami, A., Bidarpoor, F., 2014. Effects of dust storm events on emergency admissions for cardiovascular and respiratory diseases in Sanandaj, Iran. J. Environ. Health Sci. Eng. 12, 110.
Esmaili, O., Tajrishy, M., Arasteh, P.D., 2006. Evaluation of dust sources in Iran through remote sensing and synoptical analysis. Atlantic Eur. Conf. Remote Imaging Spectrosc., 136–143
Furman, H.K.H., 2003. Dust storms in the Middle East: sources of origin and their temporal characteristics. Indoor Built Environ. 12, 419–426.
Gerivani, H., Lashkaripour, G.R., Ghafoori, M., 2011. The source of dust storm in Iran a case study based on geological information and rainfall data. Carpathian J. Earth Environ. Sci. 6.
Ginoux, P., Torres, O., 2003. Empirical TOMS index for dust aerosol: applications to model validation and source characterization. J. Geophys. Res.: Atmos. 108.
Ginoux, P., Prospero, J.M., Gill, T.E., Hsu, N.C., Zhao, M., 2012. Global-scale attribution of anthropogenic and natural dust sources and their emission rates based on MODIS Deep Blue aerosol products. Rev. Geophys. 50.
Goudie, A.S., Middleton, N.J., 2000. Dust storms in south west Asia. Acta Univ. C., 73–83, Supplement
Goudie, A., Middleton, N.J., 2006. Desert Dust in the Global System. Springer Science and Business Media.
Grell, G.A., Peckham, S.E., Schmitz, R., McKeen, S.A., Frost, G., Skamarock, W.C., Eder, B., 2005. Fully coupled "online" chemistry within the WRF model. Atmos. Environ. 39, 6957–6975.
Haimberger, L., 2007. Homogenization of radiosonde temperature time series using innovation statistics. J. Clim. 20, 1377–1403.
Haimberger, L., Tavolato, C., Sperka, S., 2012. Homogenization of the global radiosonde temperature dataset through combined comparison with reanalysis background series and neighboring stations. J. Clim. 25, 8108–8131.
Hamidi, M., Kavianpour, M.R., Shao, Y., 2013. Synoptic analysis of dust storms in the Middle East. Asia-Pac. J. Atmos. Sci. 49, 279–286.
Hsu, N.C., Tsay, S.-C., King, M.D., Herman, J.R., 2004. Aerosol properties over bright-reflecting source regions. Geoscience and Remote Sensing, IEEE Transactions on 42, 557–569.
Hsu, N., Gautam, R., Sayer, A., Bettenhausen, C., Li, C., Jeong, M., Tsay, S.-C., Holben, B., 2012. Global and regional trends of aerosol optical depth over land and ocean using SeaWiFS measurements from 1997 to 2010. Atmos. Chem. Phys. Discuss. 12, 8465–8501.
Jish Prakash, P., Stenchikov, G., Kalenderski, S., Osipov, S., Bangalath, H., 2014. The impact of dust storms on the Arabian Peninsula and the Red Sea. Atmospheric Chemistry & Physics Discussions 14, 19181–19245.
Karimi, N., Moridnejad, A., Golian, S., Vali Samani, J.M., Karimi, D., Javadi, S., 2012. Comparison of dust source identification techniques over land in the Middle East region using MODIS data. Canadian J. Remote Sens. 38, 586–599.
Ke-Yi, C., 2010. The northern path of Asian dust transport from the Gobi desert to North America. Atmos. Oceanic Sci. Lett. 3, 155–159.
Kiss, P., Janosi, I., Torres, O., 2007. Early calibration problems detected in TOMS Earth-Probe aerosol signal. Geophys. Res. Lett. 34.
Lyles, M., Fredrickson, H., Bednar, A., Fannin, H., Griffin, D., Sobecki, T., 2012. Medical geology in the Middle East: potential health risks from mineralized dust exposure. EGU Gen. Assembly Conf. Abstr., 1668
Ma, X., Bartlett, K., Harmon, K., Yu, F., 2013. Comparison of AOD between CALIPSO and MODIS: significant differences over major dust and biomass burning regions. Atmos. Meas. Tech. 6, 2391–2401.
Mahowald, N.M., Dufresne, J.L., 2004. Sensitivity of TOMS aerosol index to boundary layer height: Implications for detection of mineral aerosol sources. Geophys. Res. Lett. 31.
Mears, C.A., Schabel, M.C., Wentz, F.J., 2003. A reanalysis of the MSU channel 2 tropospheric temperature record. J. Clim. 16, 3650–3664.
Moridnejad, A., Karimi, N., Ariya, P.A., 2015a. A new inventory for middle east dust source points. Environ. Monit. Assess. 187, 1–11.
Moridnejad, A., Karimi, N., Ariya, P.A., 2015b. Newly desertified regions in Iraq and its surrounding areas: Significant novel sources of global dust particles. J. Arid Environ. 116, 1–10.
Notaro, M., Yu, Y., Kalashnikova, O.V., 2015. Regime shift in Arabian dust activity, triggered by persistent Fertile Crescent drought. J. Geophys. Res.: Atmos. 120.

Prospero, J.M., Ginoux, P., Torres, O., Nicholson, S.E., Gill, T.E., 2002. Environmental characterization of global sources of atmospheric soil dust identified with the Nimbus 7 Total Ozone Mapping Spectrometer (TOMS) absorbing aerosol product. Rev. Geophys. 40, 2-1-2-31.

Rashki, A., Kaskaoutis, D., Francois, P., Kosmopoulos, P., Legrand, M., 2015. Dust-storm dynamics over Sistan region, Iran: seasonality, transport characteristics and affected areas. Aeolian Res. 16, 35–48.

Rezazadeh, M., Irannejad, P., Shao, Y., 2013. Climatology of the Middle East dust events. Aeolian Res. 10, 103–109.

Shao, Y., Wyrwoll, K.-H., Chappell, A., Huang, J., Lin, Z., McTainsh, G.H., Mikami, M., Tanaka, T.Y., Wang, X., Yoon, S., 2011. Dust cycle: An emerging core theme in Earth system science. Aeolian Research 2, 181–204.

Strachan, J., 2005. Winds of the world. Weather 60, 331–332.

Taghavi, F., Asadi, A., 2007. The Persian Gulf 12th April 2007 dust storm: observation and model analysis.

Torres, O., Bhartia, P., Herman, J., Ahmad, Z., Gleason, J., 1998. Derivation of aerosol properties from satellite measurements of backscattered ultraviolet radiation: theoretical basis. J. Geophys. Res.: Atmos. 103, 17099–17110.

Trigo, R.M., Gouveia, C.M., Barriopedro, D., 2010. The intense 2007–2009 drought in the Fertile Crescent: Impacts and associated atmospheric circulation. Agric. For. Meteorol. 150, 1245–1257.

Vasilkov, A., Joiner, J., Spurr, R., Bhartia, P.K., Levelt, P., Stephens, G., 2008. Evaluation of the OMI cloud pressures derived from rotational Raman scattering by comparisons with other satellite data and radiative transfer simulations. Journal of Geophysical Research: Atmospheres 113.

Venema, V.K., Mestre, O., Aguilar, E., Auer, I., Guijarro, J.A., Domonkos, P., Vertacnik, G., Szentimrey, T., Stepanek, P., Zahradnicek, P., 2012. Benchmarking homogenization algorithms for monthly data. Clim. Past 8, 89–115.

WMO 2011. Manual on Codes. I.1.